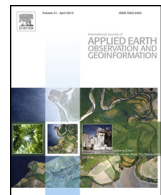




Contents lists available at ScienceDirect

# International Journal of Applied Earth Observation and Geoinformation

journal homepage: [www.elsevier.com/locate/jag](http://www.elsevier.com/locate/jag)



## Obtaining biophysical measurements of woody vegetation from high resolution digital aerial photography in tropical and arid environments: Northern Territory, Australia



G.W. Staben<sup>a,b,\*</sup>, A. Lucieer<sup>b</sup>, K.G. Evans<sup>c</sup>, P. Scarth<sup>d,e</sup>, G.D. Cook<sup>f</sup>

<sup>a</sup> Department of Land Resource Management, Northern Territory Government, PO Box 496, Palmerston Northern Territory, 0831, Australia

<sup>b</sup> School of Land and Food, University of Tasmania, Private Bag 76, Hobart, Tasmania 7001, Australia

<sup>c</sup> School of Engineering and Information Technology, Charles Darwin University, Darwin NT, 0909, Australia

<sup>d</sup> Joint Remote Sensing Research Program, School of Geography, Planning and Environmental Management, University of Queensland, St. Lucia, QLD 4072, Australia

<sup>e</sup> Remote Sensing Centre, Science Delivery, Department of Science, Information Technology, Innovation and the Arts, 41 Boggo Road, QLD 4102, Australia

<sup>f</sup> CSIRO Ecosystem Sciences, PMB 44, Winnellie, Northern Territory, 0822, Australia

### ARTICLE INFO

#### Article history:

Received 7 April 2015

Received in revised form 22 May 2016

Accepted 9 June 2016

Available online 29 June 2016

#### Keywords:

Digital aerial photography

Object-based image analysis

Foliage projective cover

Stand basal area

### ABSTRACT

Biophysical parameters obtained from woody vegetation are commonly measured using field based techniques which require significant investment in resources. Quantitative measurements of woody vegetation provide important information for ecological studies investigating landscape change. The fine spatial resolution of aerial photography enables identification of features such as trees and shrubs. Improvements in spatial and spectral resolution of digital aerial photographic sensors have increased the possibility of using these data in quantitative remote sensing. Obtaining biophysical measurements from aerial photography has the potential to enable it to be used as a surrogate for the collection of field data. In this study quantitative measurements obtained from digital aerial photography captured at ground sampling distance (GSD) of 15 cm ( $n=50$ ) and 30 cm ( $n=52$ ) were compared to woody biophysical parameters measured from 1 ha field plots. Supervised classification of the aerial photography using object based image analysis was used to quantify woody and non-woody vegetation components in the imagery. There was a high correlation ( $r \geq 0.92$ ) between all field measured woody canopy parameters and aerial derived green woody cover measurements, however only foliage projective cover (FPC) was found to be statistically significant (paired *t*-test;  $\alpha = 0.01$ ). There was no significant difference between measurements derived from imagery captured at either GSD of 15 cm and 30 cm over the same field site ( $n = 20$ ). Live stand basal area (SBA) ( $m^2 \text{ ha}^{-1}$ ) was predicted from the aerial photographs by applying an allometric equation developed between field-measured live SBA and woody FPC. The results show that there was very little difference between live SBA predicted from FPC measured in the field or from aerial photography. The results of this study show that accurate woody biophysical parameters can be obtained from aerial photography from a range of woody vegetation communities across the Northern Territory.

Crown Copyright © 2016 Published by Elsevier B.V. All rights reserved.

### 1. Introduction

Biophysical parameters obtained from woody vegetation such as stand basal area, canopy cover and foliage projective cover are important information for studies investigating landscape change (Armston et al., 2013; Clewley et al., 2012). These attributes are commonly measured in the field and have been used extensively

in ecological studies (Cook et al., 2005; Williams et al., 1997), for forest inventories (Wulder et al., 2008), and monitoring mine rehabilitation (Ludwig et al., 2003). A number of studies have shown that biophysical parameters from woody vegetation can be derived from aerial photography with reasonable levels of accuracy (Sharp and Bowman, 2004; Fensham et al., 2007; Fensham and Fairfax, 2007; Browning et al., 2009; Laliberte et al., 2010). Aerial photography represents one of the earliest forms of remote sensing and its use has been diverse (Campbell, 1996), ranging from military reconnaissance, infrastructure mapping, natural disaster management and ecosystem monitoring. It has been used in a wide range of environmental studies, with applications ranging from invasive weed

\* Corresponding author at: Department of Land Resource Management, Northern Territory Government, PO Box 496, Palmerston Northern Territory, 0831, Australia.

E-mail address: [Grant.Staben@nt.gov.au](mailto:Grant.Staben@nt.gov.au) (G.W. Staben).

mapping (Robinson et al., 2008; Dorigo et al., 2012), rangeland mapping and assessment (Laliberte et al., 2010; Browning et al., 2009; Foran and Cellier, 1980), forestry management (Coggins et al., 2008; Wulder et al., 2012) and vegetation community mapping (Harvey and Hill, 2001; Lucas et al., 2002; Lewis et al., 2013). The spatial resolution and historical record of aerial photography provide an important resource for landscape investigations (Morgan et al., 2010; Fensham and Fairfax, 2002). The fine spatial resolution (<1 m ground sampling distance) of aerial photography enables features within the landscape, such as trees and shrubs to be identified (Morgan et al., 2010). It is also used as a source of information to produce calibration and validation data for use with coarser spatial resolution satellite imagery such as Landsat suite of sensors (Mellor et al., 2013; Wulder et al., 2012; Xu et al., 2003; Congalton and Green, 2009; Coops et al., 1997; Pu et al., 2003).

The development of digital sensors has led to a marked improvement in the spatial and spectral resolution of aerial photographic imagery (Rosso et al., 2008; Wulder et al., 2012). These improvements have increased the potential use of these data for quantitative remote sensing (Laliberte et al., 2010). Coggins et al. (2008) used 10 cm ground sampling distance (GSD) digital aerial photography to extract individual tree canopy cover in forest in the Canadian Rocky Mountains. These canopy cover measurements were then related to field measured tree canopy cover and stem diameter to estimate stocking density. There was a significant correlation between estimates derived from the aerial photography and field data to enable them to be used as inputs into a model to predict the potential impacts of mountain pine beetle on these forest stands (Coggins et al., 2008; Wulder et al., 2012). Laliberte et al. (2010) used ultra-high resolution digital aerial photography (4 cm GSD) to estimate percent cover of vegetation and bare ground for a range of vegetation communities in rangelands in south-western USA. They reported high correlations between shrub, grasses and non-vegetated surfaces derived from imagery and field-based measures (Laliberte et al., 2010). One of the motivating factors for their study was to develop reliable methods which enabled the assessment of plots at an equivalent scale and detail to field-based sampling measurements, over extensive and often remote areas (Laliberte et al., 2010).

Remote sensing technology is particularly suited to the Northern Territory, due to the low population density, harsh climate and vast areas (Hill and Carter, 1999; Whiteside et al., 2011). The Northern Territory Government (NTG) is currently implementing a remote sensing monitoring program based on the Landsat suite of sensors. The temporal and spatial scale of these data has the potential to enable objective assessment of the landscape at a regional scale (Wallace et al., 2006; Karfs et al., 2009). The aim of this remote sensing program is to use quantitative information derived from both the historical archive and current Landsat imagery to monitor and assess land cover across the entire Northern Territory. This requires the development and assessment of models to predict biophysical parameters (e.g. woody cover estimates and fractional ground cover) from the suite of Landsat sensors. Studies that use coarser spatial resolution satellite imagery, such as Landsat (30 m GSD), to estimate biophysical parameters often develop predictive models by relating field measured data to the satellite imagery (Armston et al., 2009; Scarth et al., 2010). To enable these models to be developed, a sufficient quantity of field data covering the range of variability across the landscape is required. The collection of an adequate number of field sites to calibrate and validate products derived from sensors such as Landsat at a regional scale can be inhibited by both financial cost and logistical constraints (Laliberte et al., 2010; Armston et al., 2013). In addition to these constraints, assessment of the models applied to historical imagery needs to be compared to biophysical parameters measured at the time of the image capture. The level of detail within

aerial photography has enabled it to be used as a surrogate for the collection of ground data (Mannel et al., 2006). A number of studies have used aerial photography to derive biophysical parameters to calibrate Landsat satellite imagery (Xu et al., 2003; Pu et al., 2003; Carreiras et al., 2006; Samani Majd et al., 2013). Samani Majd et al. (2013) reported significant correlation between Landsat derived NDVI (normalised difference vegetation index) and fractional canopy cover measured from digital aerial photographs. In many instances, aerial photographs may be the only available data from which to assess the accuracy of results derived from coarse scale historical satellite imagery. Often when aerial photography is used to produce calibration and validation data the assumption is made that the interpretation of the aerial photographs are correct, when in fact there may be significant errors in the interpretation which remain unknown unless validation of the results are undertaken (Congalton and Green 2009).

The NTG has a large archive of aerial photographs captured since 1940s (<http://www.ntlis.nt.gov.au/imfPublic/airPhotoimf.jsp>). In 2008 the NTG moved away from the traditional film aerial photography and now routinely captures imagery using digital format cameras. The extensive archive of very high resolution digital aerial photography held by the NTG has the potential to be a valuable source of calibration and validation data for use with coarser spatial resolution sensors. The combined spatial resolution and radiometric quality of the digital sensors (Leberl et al., 2012) used to capture the imagery across the Northern Territory has the potential to enable accurate measurements of biophysical parameters from woody vegetation. The spatial extent of these data would enable a large number of surrogate field sites to be randomly generated across the Northern Territory, representing a broad range of vegetation communities. To enable these data to be used as a surrogate for field data the biophysical parameters measured need to be first extracted from the imagery, and secondly, the accuracy of the information derived needs to be quantified. The objectives of this study are: (1) develop a methodology that enables the extraction of quantitative woody vegetation biophysical parameters from very high resolution digital aerial photography, (2) statistically quantify the relationship between digital aerial photography and field measured biophysical parameters, and (3) identify and assess the effect of different GSD on the biophysical parameters extracted from digital aerial photographs. The overall aim of this study is to investigate the utility of very high resolution digital aerial photography to be used as a surrogate for the collection of field data. This paper presents the methodology developed to extract biophysical parameters from digital aerial photography captured at both 15 cm and 30 cm GSD and evaluates the accuracy of the quantitative information derived from the imagery.

## 2. Methods

### 2.1. Study area

The field sites and aerial photography used in this study are distributed across the Northern Territory of Australia (Fig. 1). The Northern Territory covers an area of 1,346,664 km<sup>2</sup>, representing approximately 16.5% of the entire Australian landmass. It is sparsely populated with most people living in the main urban centres of Darwin, Katherine and Alice Springs. The climate is varied, ranging from wet dry tropics in the north, transitioning to semi-arid and arid regions in the south (Ringrose et al., 1994). Temperatures are generally warm all year with the annual average temperature ranging from 32 °C in Darwin, 34 °C in Katherine, 32 °C in Tennant creek and 29 °C in Alice Springs. Much of the Northern Territory is influenced by a monsoonal climate with a majority of the rainfall occurring between the months of October and April

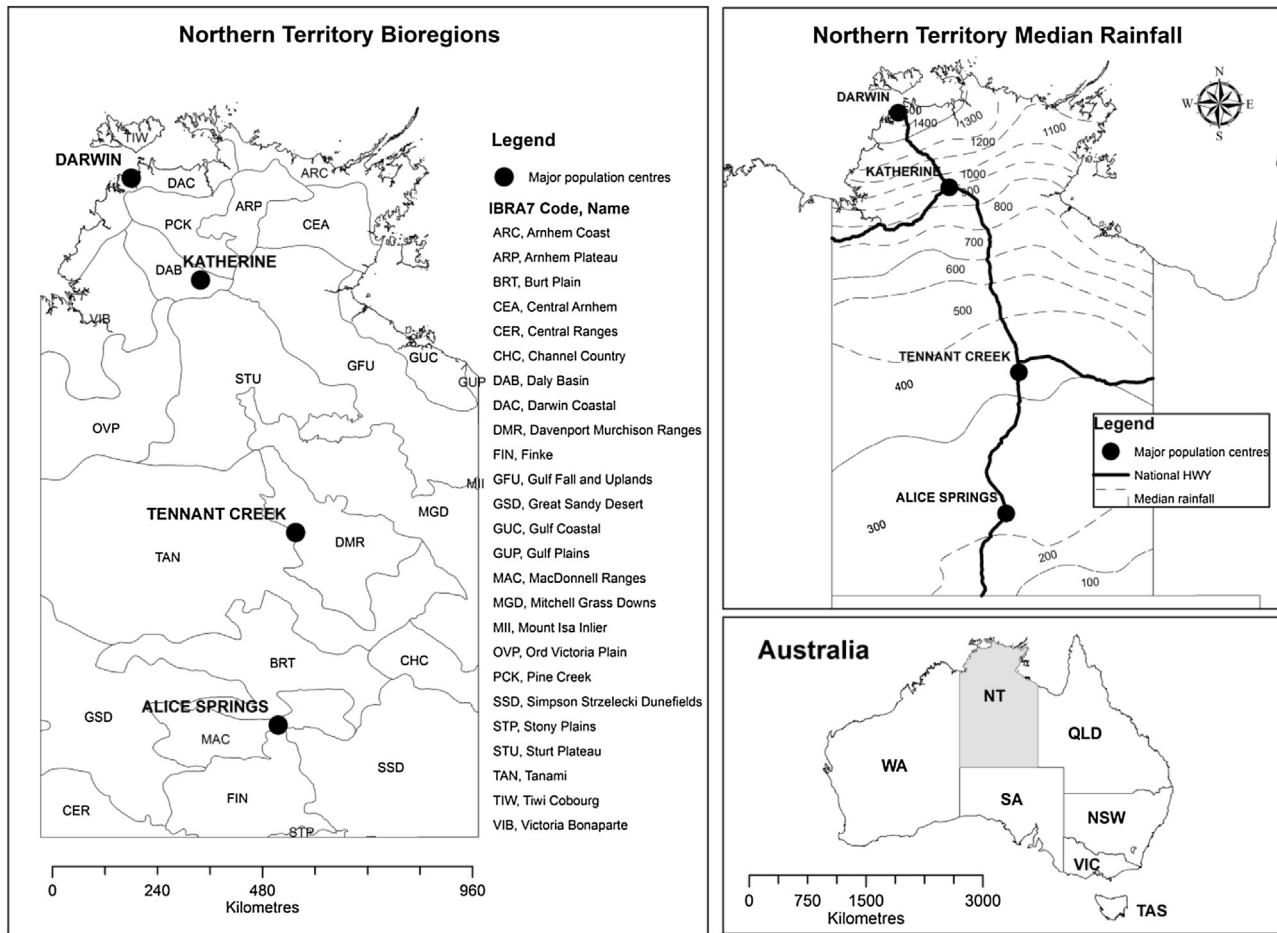


**Fig. 1.** Location of the study area Northern Territory (NT) Australia, major bioregions obtained from the Interim Biogeographic Regionalisation for Australia (IBRA) version 7 (<http://www.environment.gov.au/land/nrs/science/ibra>).

(McDonald and McAlpine, 1991). There is a distinct rainfall gradient moving south (Cook and Heerdegen, 2001) with average annual rainfall of 1729 mm recorded at Darwin airport, 1133 mm in Katherine, 474 mm for Tennant Creek and 283 mm recorded in Alice Springs ([www.bom.gov.au](http://www.bom.gov.au)).

Woody vegetation in the Northern Territory is dominated by three main Genera, *Eucalyptus* and *Corymbia* in the north transitioning to *Acacia* communities in the arid south (Wilson et al., 1990). Large areas of the northern region are dominated by *Eucalyptus tetrodonta* and *E. miniata* woodlands to open forests containing a mid-stratum of mixed semi-deciduous to deciduous trees and shrubs and grasses (Williams et al., 1997). *Melaleuca* species are found on floodplains and river systems (Franklin et al., 2007), while pockets of dry and wet rainforests are scattered across the northern half of the Northern Territory (Wilson et al., 1990). Moving south into the semi-arid regions woodlands and low open woodlands consisting of *E. tectifica*, *Corymbia terminalis* and *E. chlorophylla* are common on undulating plains and plateaux (Wilson et al., 1990). In the coastal Gulf region (Fig. 1, IBRA7 code GUC), both *E. tetrodonta* and *E. miniata* are more dominant, while *C. dichromophloia*, *E. tetrodonta* and *E. patellaris* are found on the undulating plains of the Sturt Plateau (IBRA7 code = STU). Large stands of *E. pruinosa* low woodlands are found in more poorly drained areas while *Melaleuca* woodlands are found on extensive low lying plains close to the coast (Wilson et al., 1990). Large areas of tussock grassland containing scattered trees and shrubs are found on cracking clay soils in the east (Barkly Tablelands, IBRA7 code MGD) and west (Victoria River Region, IBRA7 codes VIB, OVB). *E. microtheca* low

open woodlands are found along clay-dominated water courses and intermittent swamps on clay plains and at the southern end of the semi-arid region (Wilson et al., 1990). Toward the southern edge of the semi-arid and into the arid region *Acacia* shrublands and open-shrublands are the most common woody vegetation communities. *Acacia aneura* (mulga) is the most common woody species in this region and it is found in a wide range of habitat types (Nicholas et al., 2009; Bowman et al., 1994), with open to sparse shrublands of *A. kempanana* dominate rocky calcareous landscapes (Wilson et al., 1990). Large tracts of spinifex (*Triodia spp.*) hummock grasslands are found across the sandy plains and dune fields of the central Australian deserts (Buckley, 1981; Bowman et al., 2007). *Eucalyptus camaldulensis* is commonly found along the major sandy water courses of the semi-arid and arid zones, while in areas fringing episodic water holes *E. microtheca* and *E. camaldulensis* low open woodlands and *Melaleuca glomerata* open-shrublands are common (Wilson et al., 1990). For a more detailed review of the diverse range of vegetation communities across the Northern Territory readers are directed to Wilson et al. (1990).

## 2.2. Aerial photography

A total of 31 aerial photograph mosaics captured between the years 2010 and 2013 were used in this study. They cover a broad range of structural formations and vegetation communities ranging from monsoon rainforests, savannah woodlands dominated by *Eucalyptus* and *Corymbia* trees, Mulga woodlands, *Acacia* shrublands and *Triodia* grasslands (Fig. 2). The imagery used in



**Fig. 2.** Example of four of the sites used in this study; 15 cm GSD aerial photograph (left) and corresponding field site photograph (right); (a) Mixed species Monsoon forest, (b) *Eucalyptus miniata* and *E. tetrodonta* woodland (c) *Acacia aneura* (Mulga) woodland and (d) Sparse *Acacia* shrubland.

this project has been captured on either a Vexcel Ultracam D or Ultracam X large-format digital camera. These cameras have four

multispectral bands (red, green, blue and near infrared) and one panchromatic band, captured at 14-bit dynamic range ([Gruber](#)

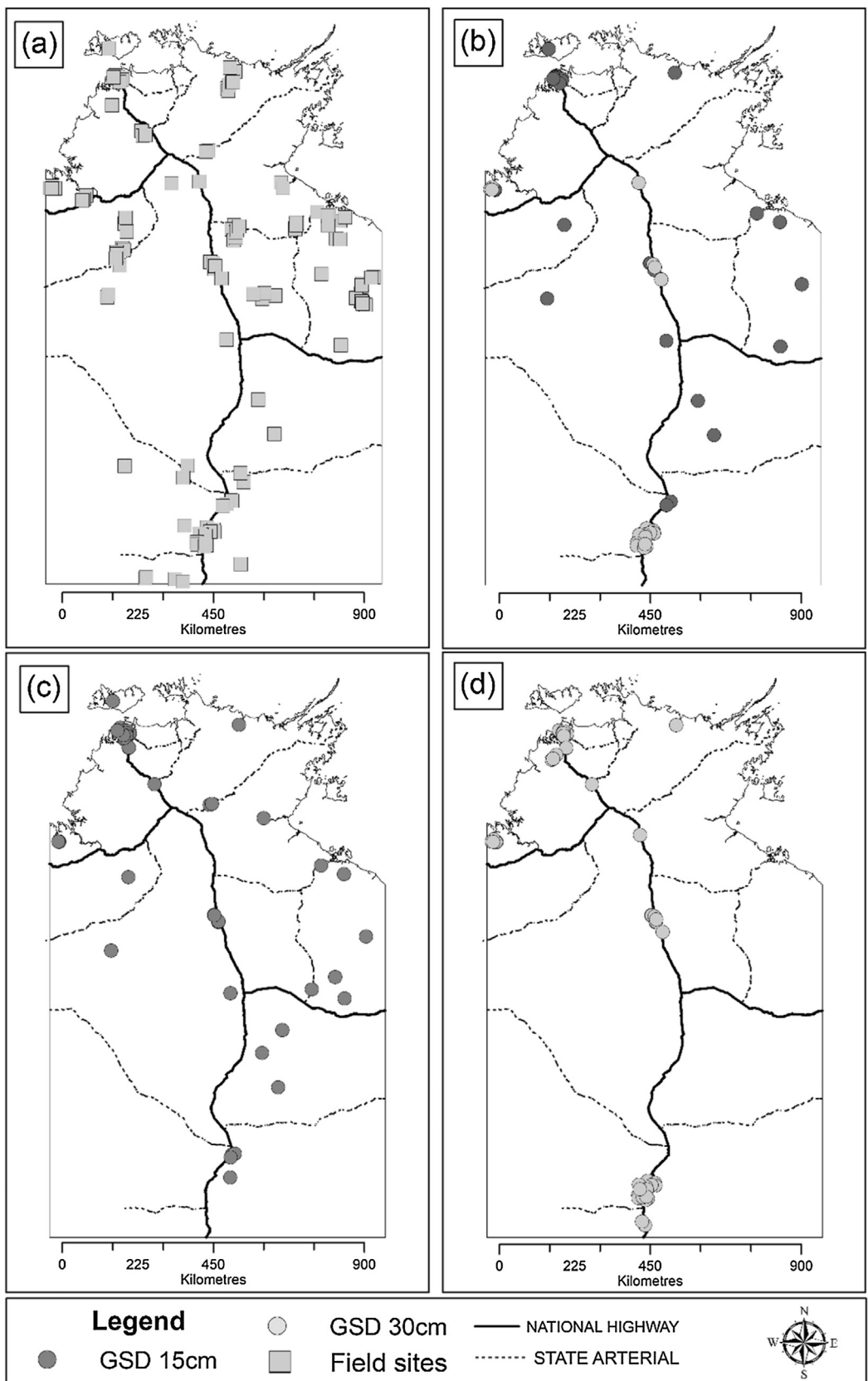


**Fig. 3.** (a) Location of all the field sites used in this study; (b) sites used to independently assess the relationship between digital aerial photography and predicted live SBA; (c) sites used to assess the relationship between tree canopy parameters and aerial photography GSD 15 cm; and (d) GSD 30 cm.

et al., 2008; Leberl and Gruber, 2005). The majority of digital aerial photography projects commissioned by the NTG are captured in the early dry season (around May–June) to reduce the impact of cloud, smoke, and haze on the imagery. To minimise the impact of shadow, imagery captured over areas with steep terrain and woody cover is restricted to times with a minimum solar altitude of 35° and for areas with open woody cover and flat terrain a minimum of 25°. Image processing is undertaken by the commercial contractors who produce a true colour (red, green, blue) orthorectified mosaic with a dynamic range of 8 bit. Imagery is supplied in a JPEG2000 compression format (10:1) with a reported spatial accuracy of <±1 m. The ground sampling distances (GSD) of imagery captured is dependent on the requirements of the project. For this study only 15 cm and 30 cm orthorectified mosaics supplied in true colour (red, green, blue) 8 bit dynamic range were available, captured between 2010 and 2013.

### 2.3. Field data

In total 168 field sites located across the Northern Territory were available for use in this study (Fig. 3a). These field sites were sampled for a variety of projects undertaken by the NTG between the years 2009 and 2013. A number of the sites used in this study were part of a network of plots, which had been re-measured between the years 2010–2013 (Cuff and Brocklehurst, 2015). In some instances the same field sites were measured on different dates, these sites were used to assess aerial photography captured at either different GSD or on different dates. Locations of field sites were selected based on a methodology developed by the NTG rangelands monitoring unit to enable these data to be used with satellite imagery, this method is based on national Australian guidelines detailed in Muir et al. (2011). Sites were located within large homogeneous patches of vegetation 100 m from any boundary effect or disturbance (Muir et al., 2011). At each field site a range of plant biophysical parameters and ground cover estimates were obtained over a 100 m × 100 m quadrat. These data were measured using a point-based intercept method which obtains measurements at 1 m intervals along three 100 m tapes configured in a star shape (Fig. 4). A densitometer sight tube (Stumpf, 1993) was used at the operator's eye height to record vertical intercepts of green leaf, dead leaf, branch, and sky within the extent of canopy for woody vegetation for the upper and mid stratum. Below the operators eye height an optical laser pointer was used to record the intercepts for woody vegetation in the ground stratum. In addition to the woody vegetation parameters, estimates of ground cover

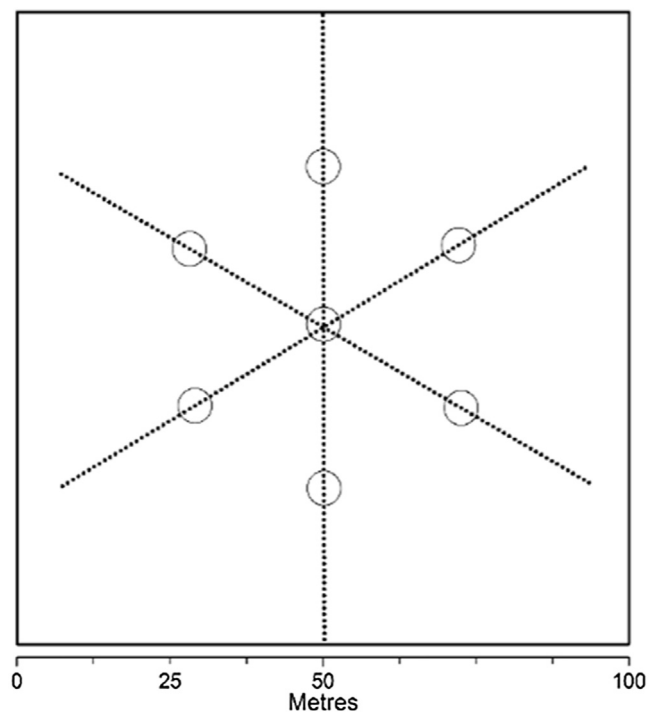


**Fig. 4.** Example of the transect configuration of a 100 m × 100 m (1 ha) field site used to collect woody cover estimates, circles denote where tree basal area measurements were collected.

were also obtained along these transects. The ground layer measurements included green and dead leaf for herbs, forbs and grasses, litter, bare ground, rock and cryptogam. Stand basal area (SBA) estimates ( $m^2 \text{ ha}^{-1}$ ) for individual woody species were also obtained for each site using a Haglöf factor gauge (Muir et al., 2011). At each site, seven individual basal sweeps were performed at pre-defined locations on the star transect (Muir et al., 2011). The mean of these measures were used to calculate the SBA ( $m^2 \text{ ha}^{-1}$ ) for live and dead trees at each site. The centre of each plot was recorded using averaged GPS readings. Averaged GPS readings were recorded during the measurement of each field site which took between 1 to 3 h.

Parameters for woody vegetation such as total canopy cover, plant projective cover and foliage projective cover for the over story, mid story and ground stratum are derived for each site. Foliage projective cover (FPC) represents the percentage of the

**Table 1**

Summary of the field sites used to investigate the relationship between tree biophysical parameters and 15 cm and 30 cm GSD aerial photographs, field sites are grouped into broad structural classes based on the National Vegetation Information System (Brocklehurst et al., 2007).

NVIS class	No. sites	Mean CC (%) (range)	Mean SBA( $m^2 \text{ ha}^{-1}$ ) (range)	No. sites 15 cm GSD	No. sites 30 cm GSD
Low isolated shrubs	8	1.2 (0.33–3.99)	0.04 (0.00–0.19)	1	7
Low isolated trees	1	3.7	0.93		1
Low open forest	1	55.0	7.46		1
Low open woodland	10	13.3 (8.65–18.33)	2.11 (1.69–3.04)	6	4
Low sparse shrubs	2	6.3 (5.66–7.00)	0.02 (0.00–0.042)	1	1
Low tussock grassland	1	0.0	0.00		1
Low woodland	13	29.5 (20.00–37.33)	3.68 (0.35–6.60)	9	4
Mid closed forest	7	94.2 (89.63–100)	26.63 (17.78–34.2)	4	3
Mid hummock grassland	2	0.0	0.00		2
Mid isolated shrubs	1	0.7	0.00		1
Mid isolated trees	2	3.5 (2.33–4.65)	0.51 (0.00–0.09)		2
Mid open forest	22	64.2 (53.00–77.99)	13.74 (5.96–20.14)	13	9
Mid open woodland	6	11.6 (5.66–17.34)	1.44 (0.03–2.64)	3	3
Mid sparse shrubland	2	6.7 (6.31–7.00)	0.02 (0.00–0.04)		2
Mid woodland	20	34.9 (21.26–49.33)	5.66 (1.37–14.93)	10	10
Tall isolated shrubland	1	0.0	0.66		1
Tall open shrubland	1	28.0	3.94		1
Tall sparse shrubland	2	10.0 (6.00–14.00)	1.41 (0.11–2.71)	1	

sample site covered by the vertical projection of green foliage for woody vegetation. In this project, three broad vegetation strata were recorded, upper, mid and ground as defined in Brocklehurst et al. (2007). The number of strata recorded was dependent on the woody vegetation structure at each site. In some instance no upper or mid stratum existed, the height of vegetation in each strata is site specific and determined by the field team at the time of data collection. This enabled the proportion of FPC to be calculated for each stratum,  $U_{FPC}$  represents FPC for the upper canopy,  $UM_{FPC}$  is the combination of the upper and mid canopy FPC and  $UMG_{FPC}$  represents the total woody FPC for the site. Plant projective cover (PPC) represents the percentage of a site which is covered by the vertical projection of both green, dead foliage (dead leaf) and branches for woody vegetation for all three strata. CC is defined as the percentage of the sample site within the periphery of the tree crown, treating the crown as opaque (Walker and Hopkins, 1990). In this study, CC represented the area of the site covered by the vertical projection of PPC and sky (canopy gaps) recorded within the crowns of woody vegetation in the upper and mid stratum.

#### 2.4. Canopy biophysical parameters and aerial photography

Of the 168 sites available, 75 were located within the extent of digital aerial photography representing a broad range of structural classes (Table 1). These 75 field sites were used to assess the relationship between aerial photography and field measured woody biophysical canopy parameters. For aerial photography captured at 15 cm GSD, 50 individual field site measurements (on different sampling dates) from 46 sites were available, while 52 individual field site measurements recorded from 50 field sites were used to assess aerial photography captured at 30 cm GSD. Twenty of the 75 field sites used in this study had aerial photography captured at both 15 cm and 30 cm GSD and were used to investigate the difference between parameters derived from aerial photography at the same field sites. The difference between the field and image capture dates used in this study are summarised in Tables 2 and 3, with 75% of field sites measured <1 year of the image capture.

**Table 2**

Summary statistics for the number of days between the field and image capture dates for the 15 cm GSD aerial photography.

15 cm	<1 year	1–2 years	2–3 years
n sites	34	10	6
min (days)	9	373	737
max (days)	350	493	1093
mean (days)	120	413	837

**Table 3**

Summary statistics for the number of days between the field and image capture dates for the 30 cm GSD aerial photography.

30 cm	<1 year	1–2 years	2–3 years	4–5 years
n sites	43	3	5	1
min (days)	24	735	770	1477
max (days)	342	736	783	1477
mean (days)	143	735	776	

#### 2.4.1. Classification of aerial photographs

For each of the field sites a 100 m × 100 m subset was extracted from the digital aerial photo mosaic and classification of these data was performed using an object based image analysis (OBIA) approach in eCognition® Developer 8. A ruleset was developed that first segmented the image into meaningfully sized objects and then classified the image using a supervised nearest neighbour classification algorithm (Fig. 5). This studies area of interest encompasses a broad range of vegetation communities from the wet-dry tropics to the arid deserts of interior Australia. The digital number values representing green vegetation for the different vegetation communities across the NT were highly variable (see Fig. 2). Classification of imagery using an OBIA approach has been shown to reduce the salt and pepper effect in the imagery and increase accuracy of the classification over a per-pixel approach in northern Australia (Whiteside et al., 2011). Coggins et al. (2008) successfully used an OBIA supervised classification approach to obtain tree crown areas from aerial photography. Laliberte et al. (2010) developed an OBIA hierarchical classification approach which used a combination of rule based

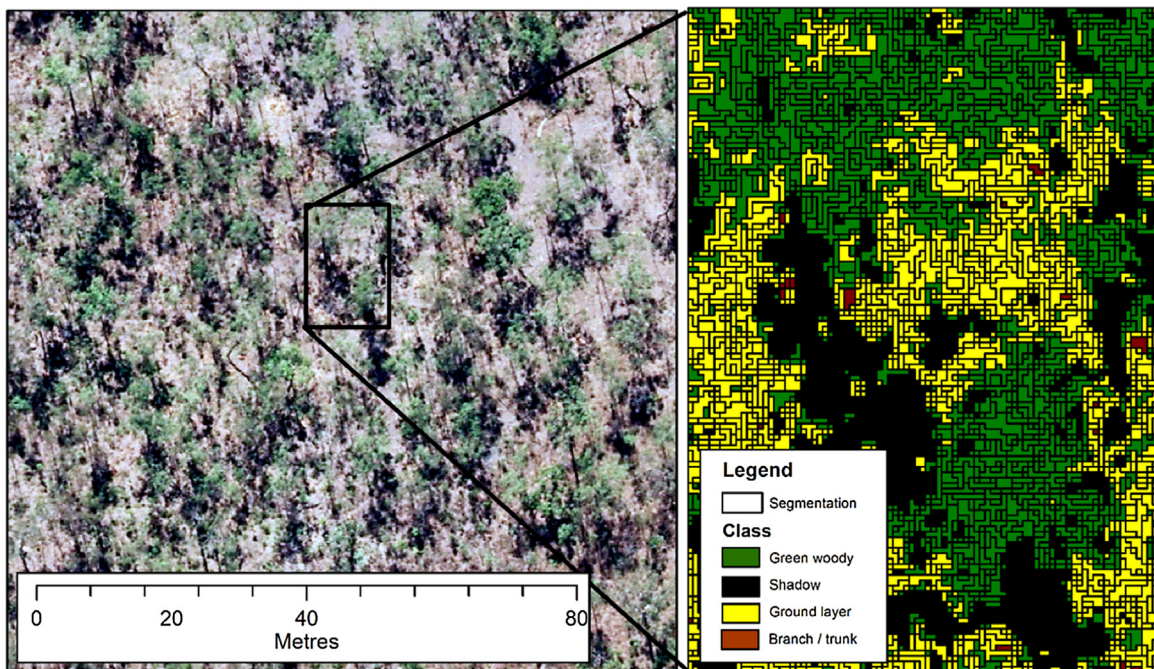


**Fig. 5.** Example of the segmentation and classification of 15 cm digital aerial photography, showing that objects produced from the fine segmentation of the imagery which enable gaps in the tree canopy to be identified and classified.

**Table 4**

Example of the summary statistic for objects derived in the segmentation process and the number of objects used for the training of each class for sites shown in Fig. 2. The letter in brackets in the site column corresponds to the 15 cm aerial photograph shown in Fig. 2 and for two sites (a) and (b) where both GSD were captured the summary statistics for 30 cm imagery are also shown.

Site	GSD	Image Objects statistics				Training samples per class (no. objects)				
		Total no.	Min no. pixels	Max no. pixels	Mean (SD) no. pixels	Green woody	Ground	Shadow	Trunk Branch	Green grass
HJ (a)	15 cm	168652	1	32	2.64 (2.37)	1587	–	35	7	–
HJ	30 cm	37067	1	35	3.00 (2.62)	81	–	19	5	–
HOW (b)	15 cm	152203	1	32	2.92 (2.64)	981	555	151	6	–
HOW	30 cm	54740	1	20	2.03 (1.59)	71	211	47	–	–
MURR (c)	15 cm	136948	1	40	3.48 (3.13)	67	1256	129	8	40
EPA (d)	15 cm	130327	1	50	3.63 (3.29)	136	2748	56	–	–

and supervised nearest neighbour algorithm to successfully classify ultra-high resolution aerial photography. They used the nearest neighbour algorithm to classify the image at the finer scale level as it enabled them to take into account the spectral variability of target objects in different images (Laliberte et al., 2010). The OBIA supervised classification method used in this study enables the user to rapidly train the classification algorithm taking into account the specific spectral variability within each aerial photograph subset. For a comprehensive review of OBIA readers are referred to Blaschke (2010) and Blaschke et al. (2014).

#### 2.4.2. Segmentation

The multi-resolution segmentation algorithm used by eCognition is a bottom-up region merging technique, starting with single pixel objects. During the hierarchical segmentation smaller image objects are merged into larger ones, based on unit-less parameters scale, colour and shape (Benz et al., 2004). These parameters define the growth in heterogeneity between adjacent image objects and this iterative process stops once the smallest growth exceeds the threshold defined by the scale parameter (Laliberte et al., 2007). To define the segmentation parameter a number of different values were assessed to determine the optimal segmentation of the aerial photography for both GSD. This is a subjective process which relies on the operator's expert knowledge to select parameters that produce objects at a meaningful size. The main objective of this study was to identify green woody vegetation cover in a broad range of vegetation communities. Thus the final parameters for the segmentation of the 15 and 30 cm aerial photographs were chosen to reduce the spectral heterogeneity in the image while still retaining enough detail to identify gaps in individual tree canopies. The final parameters selected for the segmentation of both the 15 cm and 30 cm imagery were; scale 3, colour and shape 0.9/0.1 and smoothness/compactness 0.5/0.5 respectively. All three spectral bands were weighted evenly (weight value = 1) in the segmentation. An example of the number of objects and summary statistics for the aerial photographs for field sites shown in Fig. 2 are detailed in Table 4.

#### 2.4.3. Classification

The supervised nearest neighbour classification algorithm used in this study returns a value for each object indicating the probability of belonging to a certain class. If an object is identical to a sample it is given a value of one, while objects different from a sample are assigned a value between zero and one based on a fuzzy dependency of the feature space distance to the nearest sample of a class (Trimble, 2013). The user determines both the number of classes used in the classification and the features used to define the feature space. A large number of statistics describing colour, shape and texture characteristics derived from the image objects are available to define the feature space used in the classification (Blaschke, 2010). In this study, only the mean digital numbers from each band were used to define the feature space used in the classification. For the majority of the aerial photograph subsets four main

classes were defined (1) green woody vegetation, (2) branches or trunks, (3) shadow and (4) ground layer. Due to the dry season conditions at the time of a majority of the image capture dates, the ground layer class usually consisted of either bare ground or non-green vegetation. In some instances where the ground stratum had green grass present, a fifth class (green grass) was added to the classification to reduce confusion between green woody and no-woody vegetation. For each aerial photograph subset, samples were selected from across the image to train each of the classes. The number of training samples per class varied (see Table 4 for an example) and was dependent on the area covered by the particular class in the aerial photograph. On average about 1% of the total objects were selected as training objects to classify each aerial photograph subset. It took between 20 and 30 min to process each aerial photo subset this included extracting the 100 m × 100 m subset from the aerial photo mosaic, selecting the training samples for each class and running the classification and exporting the results.

The results of the classification were exported to enable accuracy assessment of the classification and identify the proportion of area ( $m^2$ ) for each class. The area attributed to the green woody vegetation class ( $AP_{GWC}$ ) was used to estimate the percentage green woody cover for each 1 ha site. The green woody cover estimates derived from each of the aerial photograph subsets were then compared with the field measured tree biophysical parameters CC, PPC,  $U_{PPC}$ ,  $UM_{PPC}$  and  $UMG_{PPC}$  to identify any relationships between the estimates of  $AP_{GWC}$  obtained from the digital aerial photography. The  $AP_{GWC}$  estimates derived from the aerial photographs were also used to predict live woody SBA for each of the plots.

#### 2.5. Classification method accuracy assessment

In order to assess the performance of the classifier's ability to predict the desired classes based on the training data, a test was undertaken to understand the classifier commission and omission error when used on novel data that were not used in the formation of the algorithm. This tests how well the method generalises to new examples from the same data domain (Baldi et al., 2000). This test requires the same expert operator who collected the training data to undertake labelling of additional random samples across the RGB digital aerial photograph.

Assessment of the accuracy of the classified aerial photographs was undertaken on a subset (30) of the 96 sites used in this study. Fifteen sites were randomly selected to represent each spatial resolution (GSD 15 cm and 30 cm). To produce a reference dataset to evaluate the classification, 200 points were randomly generated in a GIS for each of the 30 aerial photographs and overlayed on the 100 m × 100 m RGB aerial photograph subset. The 200 points were visually evaluated and assigned to one of the five classes used in the classification and the point vector files were then intersected with the corresponding classified image to produce the accuracy statistics. The results were then pooled into their respective GSD categories (15 cm = 3000 points, 30 cm = 3000 points) to calculate the producer (commission error) and user accuracy (omis-

**Table 5**

Overall classification accuracy for the 15 randomly selected aerial photographs captured at 15 cm (GSD), along with the NVIS structural class, broad climatic zone and dominant vegetation species taken from the field data.

NVIS class	Broad climate Zone	Dominant vegetation species	Overall accuracy
Low open woodland	Semi-arid	<i>Lophostemon lactifluus/Acacia auriculiformis</i>	81.5
Low woodland	Semi-arid	<i>Eucalyptus tetrodonta</i>	82.5
Low woodland	Humid	<i>Acacia estrophialata</i>	81.5
Low woodland	Arid	<i>Eucalyptus tetrodonta/Eucalyptus miniata</i>	70.0
Mid closed forest	Humid	<i>Eucalyptus tectifica</i>	89.0
Mid closed forest	Humid	<i>Bauhinia cunninghamii</i>	80.0
Mid open Forest	Humid	<i>Erythrophleum chlorostachys/Corymbia polycsiada</i>	80.5
Mid open forest	Humid	<i>Callitris intratropica</i>	77.0
Mid open forest	Humid	<i>Eucalyptus tetrodonta/Eucalyptus miniata</i>	69.5
Mid open woodland	Arid	<i>Corymbia opaca/Acacia coriacea</i>	80.0
Mid woodland	Semi-arid	<i>Eucalyptus tetrodonta/Eucalyptus miniata</i>	88.5
Mid woodland	Humid	<i>Eucalyptus tetrodonta/Eucalyptus miniata</i>	84.0
Mid woodland	Semi-arid	<i>Eucalyptus tetrodonta/Eucalyptus miniata</i>	79.5
Mid woodland	Humid	<i>Corymbia dichromophloia</i>	71.5
Tall sparse shrubland	Arid	<i>Eucalyptus tetrodonta/Eucalyptus miniata</i>	87.0

Broad climatic zones are defined by the median rainfall (Fig. 1), Humid zone > 1000 mm, Semi-arid zone 500–1000 mm and Arid zone < 500 mm.

sion error) for each class and the overall accuracy, which were presented in a standard error matrix (Congalton and Green, 2009).

## 2.6. Stand basal area and aerial photography

An allometric relationship between coincident field-measured UMG<sub>FPC</sub> and live stand basal area (SBA) measurements was developed from 127 sites across the Northern Territory. This allometric relationship was developed using a non-linear power function based on a robust regression technique:

$$\text{livesba} = a \times x^b + c \times x^d \quad (1)$$

where  $a$ ,  $b$ ,  $c$ , and  $d$  are the best fit parameters and  $x$  is the field measured UMG<sub>FPC</sub>. The field-based allometric relationship was then applied to estimates of AP<sub>GWC</sub> derived from aerial photography, captured at 15 cm and 30 cm GSD to predict live SBA. A robust regression technique was chosen as the independent variables (field measured UMG<sub>FPC</sub>) would not be free of measurement error and robust regression techniques are less impacted by outliers (Cohen et al., 2003)

To independently assess the live SBA estimates derived from the aerial photography, 50 of the 168 field sites available in this study were not used in the development of the allometric equation. Forty four of the 50 sites were randomly selected from the 75 sites used in the assessment of canopy biophysical parameters and aerial photography. These 44 randomly selected sites contained both field measured UMG<sub>FPC</sub> and live SBA, while only live SBA measurements were recorded during the field surveys at the remaining six sites. The allometric equation developed in this study was applied to field measured UMG<sub>FPC</sub> ( $n=44$ ) and AP<sub>GWC</sub> ( $n=50$ ) obtained from the independent sites.

## 2.7. Statistical analysis of relationship between field biophysical parameters and AP<sub>GWC</sub>

The assumption in this study was that field measured biophysical parameters represent the accurate measure of these parameters at each location. A number of statistics were used to identify and assess the relationships between measures derived from the aerial photographs and the field woody vegetation cover and live SBA measures. Pearson's product moment correlation coefficient (Zar, 1984) was used to assess the correlation between the field-based biophysical parameters and photo-derived green woody cover and predicted live SBA. The root mean square error (RMSE) (Congalton and Green, 2009) was used to assess the overall error (difference) between the field-measured biophysical parameters and the

photo-derived estimates. Variance was used to assess the precision of the biophysical estimates from the aerial photography and the field-measured estimates. Bias was calculated to assess the average difference between the photo-derived and field-measured parameters and indicates the dispersion of data around the one-to-one line. To determine if there were statistically significant differences between AP<sub>GWC</sub> derived from aerial photography and the field-measured biophysical parameters (CC, PPC, U<sub>FPC</sub>, UM<sub>FPC</sub>, UMG<sub>FPC</sub>, live SBA) a paired *t*-test was used with a confidence level of 99% (Zar, 1984).

## 3. Results

### 3.1. Classification accuracy assessment

The results of the accuracy assessment of the classified aerial photographs are presented in Tables 5, 6, 7 and 8. For sites captured at 15 cm GSD the minimum individual accuracy was 69.5%, this occurred in a *Eucalyptus tetrodonta* and *Euc miniata* open forest site located in the north half of the NT. The site with the highest accuracy (89%) occurred in a site dominated by *Eucalyptus tectifica* also located in the northern half of the NT. The overall accuracy for the 15 cm imagery was 80%, with the highest individual accuracy for the ground layer class. For the green woody vegetation class (the focus of this study) the producer and user accuracy was similar to the overall accuracy (~80%), with the majority of the commission and omission error between the ground layer and shadow classes. While there was minor omission and commission error between the green grass and branch/trunk class and green woody vegetation. The producer and user accuracy for the branch & trunk class was very low with commission error between the green woody vegetation, ground layer and shadow classes. Producer's accuracy for the green grass class was low with commission error between green woody vegetation and ground layer class, and omission error occurring as a result of confusion with the ground layer, shadow and green woody vegetation classes.

For the 30 cm classification accuracy the lowest value (74.5%) occurred in a site located in the semi-arid zone dominated by the species *Bauhinia cunninghamii*. The highest accuracy (97%) occurred in two sites located in the arid zone. The accuracy for the classification for sites at 30 cm GSD was higher than the 15 cm imagery with an overall accuracy of 86%. While overall accuracy was higher than the 15 cm imagery the users and producers accuracy for the green woody vegetation class for 30 cm imagery was slightly lower. As with the results of the 15 cm classification most of the omission and commission error for the green woody vegetation class occurred

**Table 6**

Overall classification accuracy for the 15 randomly selected aerial photographs captured at 30 cm (GSD) along with the NVIS structural class, broad climatic zone and dominant tree species taken from the field data.

NVIS class	Broad climate Zone	Dominant vegetation species	Overall accuracy
Low isolated shrubs	Arid	<i>Acacia kempeana</i>	90.0
Low isolated shrubs	Arid	<i>Acacia aneura/Eremophila spp</i>	89.5
Low isolated shrubs	Arid	<i>Sclerolaena laniscuspis/Enneapogon polypyllus</i>	77.5
Low isolated trees	Arid	<i>Corymbia terminalis</i>	77.0
Low open forest	Semi-arid	<i>Eucalyptus tetrodonta/Eucalyptus miniata</i>	82.0
Low open woodland	Arid	<i>Acacia aneura/Senna spp</i>	79.0
Low open woodland	Semi-arid	<i>Bauhinia cunninghamii</i>	74.5
Mid closed forest	Humid	<i>Acacia auriculiformis/Carpentaria acuminata</i>	85.0
Mid isolated shrubs	Arid	<i>Eremophila duttonii</i>	97.0
Mid isolated trees	Humid	<i>Corymbia polycarpa</i>	92.5
Mid open woodland	Arid	<i>Eucalyptus microtheca</i>	93.5
Mid sparse shrubland	Arid	<i>Acacia aneura/Acacia kempeana</i>	97.0
Mid sparse shrubland	Arid	<i>Acacia kempeana</i>	90.0
Mid woodland	Arid	<i>Acacia aneura</i>	89.5
Mid woodland	Humid	<i>Eucalyptus tetrodonta/Eucalyptus miniata</i>	77.5

Broad climatic zones are defined by the median rainfall (Fig. 1), Humid zone > 1000 mm, Semi-arid zone 500–1000 mm and Arid zone < 500 mm.

**Table 7**

Error matrix showing the accuracy assessment results for the classification of 15 cm GSD digital aerial photography (n = 15 sites).

Classified data	Reference data						Users accuracy
	Green woody	Shadow	Ground layer	Branches & trunks	Green grass	Total	
Green woody	726	72	100	4	12	914	79.4%
Shadow	97	389	48	1	0	535	72.7%
Ground layer	99	103	1232	3	8	1445	85.3%
Branches & trunks	1	0	5	1	0	7	14.3%
Green grass	6	16	22	0	55	99	55.6%
Total	929	580	1407	9	75	3000	
Producers accuracy	78.1%	67.1%	87.6%	11.1%	73.3%		

Overall accuracy = 80.1%.

**Table 8**

Error matrix showing the accuracy assessment results for the classification of 30 cm GSD digital aerial photography (n = 15 sites).

Classified data	Reference data						Users accuracy
	Green woody	Shadow	Ground layer	Branches & trunks	Green grass	Total	
Green woody	306	51	57	0	3	417	73.4%
Shadow	60	220	23	0	5	308	71.4%
Ground layer	39	75	1942	0	26	2082	93.3%
Branches & trunks	3	0	0	0	0	3	0.0%
Green grass	6	17	52	0	115	190	60.5%
Total	436	345	2070	0	149	3000	
Producers accuracy	73.9%	60.6%	93.6%	0.0%	77.2%		

Overall accuracy = 86.1%.

between the shadow and ground layer classes. The accuracy of the ground layer was high with most omission and commission error between the green woody vegetation, shadow and green grass classes. For the green grass class most omission and commission error occurred with the ground layer class. The branch & trunk class was not assessed as none were identified during the visual assessment of the 3000 randomly selected points.

### 3.2. Relationship between field biophysical parameters and AP<sub>GWC</sub>

3.2.1. 15 cm aerial photography

The results show that there is a significant correlation between the field measured cover parameters ( $U_{FPC}$ ,  $UM_{FPC}$ ,  $UMG_{FPC}$ , PPC, CC) and 15 cm aerial derived AP<sub>GWC</sub> estimates (n = 50) (Fig. 6, Table 9). Field-measured  $U_{FPC}$  and  $UM_{FPC}$  were overestimated by AP<sub>GWC</sub> and conversely PPC and CC were underestimated (Fig. 6). The lowest RMSE value was found between  $UMG_{FPC}$  and AP<sub>GWC</sub> while the variance was slightly lower between  $UM_{FPC}$  and AP<sub>GWC</sub>. The lowest bias value was recorded between  $UMG_{FPC}$  and AP<sub>GWC</sub>.

**Table 9**

Results of assessment of the relationship between AP<sub>GWC</sub> estimated from 15 cm digital aerial photography and field woody cover estimates ( $U_{FPC}$ ,  $UM_{FPC}$ ,  $UMG_{FPC}$ , PPC and CC).

Woody cover parameter	r	RMSE	Variance	Bias	T statistic	P value
$U_{FPC}$	0.92	10.85	62.85	7.49	-6.68	<0.001
$UM_{FPC}$	0.95	7.28	38.17	3.94	-4.51	<0.001
$UMG_{FPC}$	0.95	6.84	47.74	0.09	0.09	0.926
PPC	0.95	8.62	52.86	-4.74	4.61	<0.001
CC	0.95	14.83	88.12	-11.56	8.71	<0.001

which is also reflected in the scatter around the 1 for 1 line (Fig. 6). A paired t-test ( $\alpha = 0.01$ ) was used to assess if there were differences in the mean values between field-based measurements and the aerial photo derived estimates (Fig. 6). The only field-based cover parameter that was not significantly different to the mean of AP<sub>GWC</sub> estimates was  $UMG_{FPC}$ .

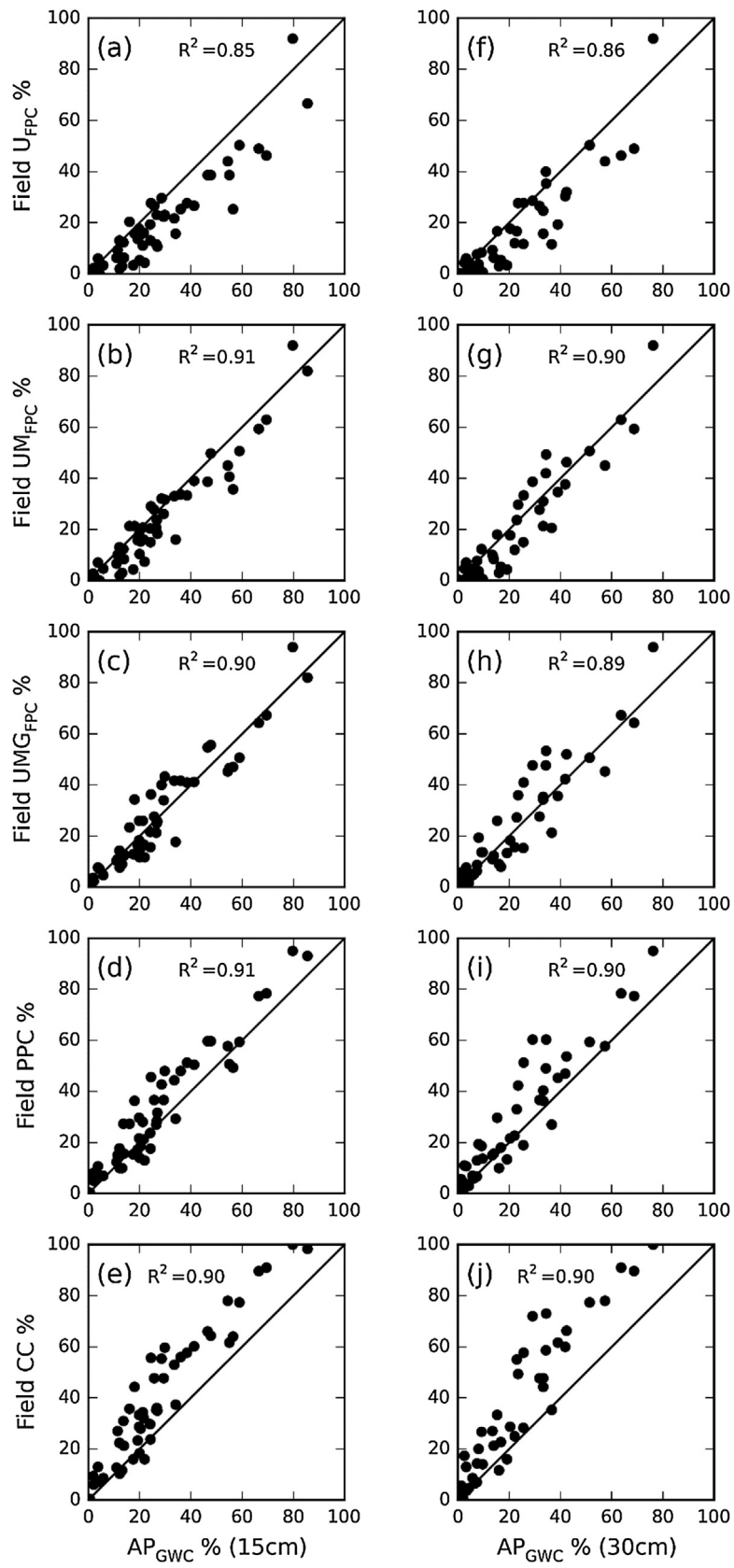


**Fig. 6.** Scatter plots showing the relationship between  $AP_{GWC}$  (x-axis) estimated from digital aerial photography captured at GSD 15 cm (a–e) and 30 cm (f–j) and field-measured  $U_{FPC}$ ,  $UM_{FPC}$ ,  $UMG_{FPC}$ , PPC and CC (y-axis), fitted line represents the 1:1 correspondence.

**Table 10**

Results of assessment of the relationship between AP<sub>GWC</sub> estimated from 30 cm digital aerial photography and field woody cover estimates (U<sub>FPC</sub>, UM<sub>FPC</sub>, UMG<sub>FPC</sub>, PPC and CC).

Woody cover parameter	r	RMSE	Variance	Bias	T statistic	P value
U <sub>FPC</sub>	0.92	8.81	56.98	4.66	-4.45	<0.001
UM <sub>FPC</sub>	0.95	6.89	44.68	1.91	-2.06	0.045
UMG <sub>FPC</sub>	0.94	7.39	53.48	-1.46	1.44	0.157
PPC	0.95	9.66	67.93	-5.16	4.51	<0.001
CC	0.95	15.88	141.14	-10.67	6.47	<0.001

### 3.2.2. 30 cm aerial photography

The results for the 30 cm imagery ( $n=52$ ) are similar to the 15 cm imagery with high correlations between all field-measured woody cover parameters and AP<sub>GWC</sub> (Fig. 6, Table 10). The scatter plots show that field measured U<sub>FPC</sub> was overestimated by AP<sub>GWC</sub>, while UM<sub>FPC</sub> and UMG<sub>FPC</sub> were scattered around the 1:1 line. Both PPC and CC were underestimated when compared to AP<sub>GWC</sub> values. Based on the r, RMSE, variance and bias statistics shown in Table 3, both UM<sub>FPC</sub> and UMG<sub>FPC</sub> had the strongest relationship with AP<sub>GWC</sub>, with UM<sub>FPC</sub> having both the lowest RMSE and variance. Results from the paired t-test ( $\alpha=0.01$ ) show that both field measured UM<sub>FPC</sub> and UMG<sub>FPC</sub> were not significantly different to the mean values of AP<sub>GWC</sub>.

### 3.3. Comparison of the results between aerial photography captured at 15 cm and 30 cm GSD

The results show that the relationship between the field measured canopy parameters and imagery was stronger for 15 cm GSD in comparison to imagery captured at 30 cm GSD (Fig. 6). Overall the variance was lower for the 15 cm data for each of the parameters assessed, which is reflected in the spread of data in Fig. 6. Variance between field tree canopy parameters for both the 15 cm and 30 cm imagery was lowest between UM<sub>FPC</sub>, however, for all other statistics the relationship was strongest with UMG<sub>FPC</sub> for both 15 cm and 30 cm GSD.

To further investigate the influence of the different GSD, comparisons were made between the AP<sub>GWC</sub> values derived from 20 field sites where both 15 cm and 30 cm aerial photographs had been captured. A paired t-test was used to investigate if there was a statistically significant difference between the AP<sub>GWC</sub> estimates derived from the two different GSD. There was a high correlation ( $r=0.94$ ) between AP<sub>GWC</sub> derived from aerial photography at GSD of 15 cm and 30 cm for most sites (Fig. 7). The results of the paired t-test indicated that there was no significant difference between the two spatial resolutions ( $T$  value = 1.35;  $P$ -value = 0.191;  $\alpha=0.01$ ). While most of these data points were close to the 1:1 line, a number of outliers were present, recording up to 22% difference in estimated AP<sub>GWC</sub> between the different GSD.

### 3.4. Stand basal area

The best fit function for the allometric relationship between field-measured UMG<sub>FPC</sub> and live SBA is shown in Fig. 8. The scatter around the best fit function highlights the variability in the relationship between UMG<sub>FPC</sub> and live SBA, with the greatest variance occurring between the ranges of 30 and 60% UMG<sub>FPC</sub>. Summary statistics for the non-linear power function and best fit parameters for the allometric equation are presented in Table 11. The allometric relationship was then applied to independent field measured UMG<sub>FPC</sub> ( $n=44$ ) and aerial photograph ( $n=50$ ) measured AP<sub>GWC</sub> to assess the accuracy of the predicted live SBA measures.

The statistics used to assess the overall accuracy based on the predicted and observed values (Table 11) show that there was little difference between the 127 sites used to define the allometric

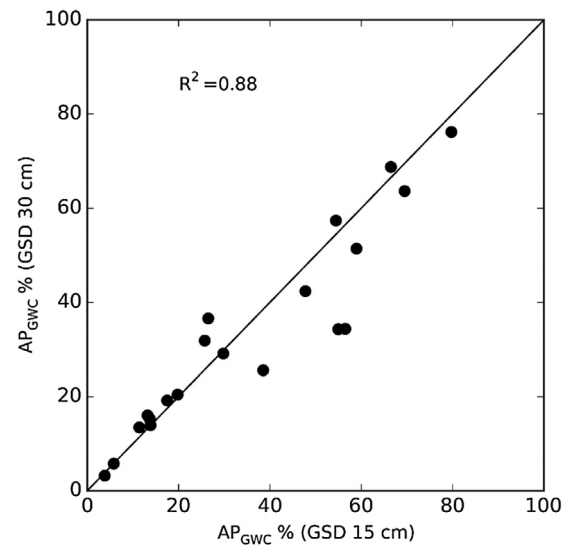


Fig. 7. Scatter plot showing the relationship between AP<sub>GWC</sub> derived from aerial photography captured at both 15 cm and 30 cm GSD for the same field site, fitted line represents the 1:1 correspondence.

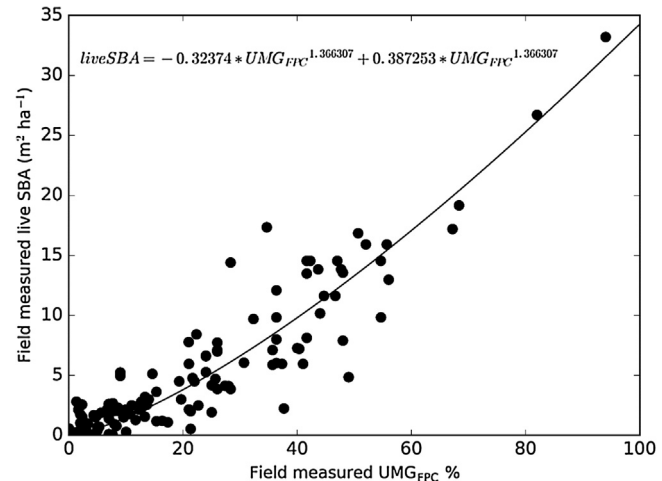


Fig. 8. Fitted line for the allometric relationship between field-measured UMG<sub>FPC</sub> and live SBA  $\text{m}^2 \text{ha}^{-1}$ ; the equation for the fitted line is shown in equation 1 (Section 2.7) and the best fit parameters are shown in Table 9.

relationship and the 50 independent sites. The predicted (Eq. (1)) and observed live SBA estimates derived from aerial photography AP<sub>GWC</sub> and field-measured UMG<sub>FPC</sub> for the independent validation sites are presented in Fig. 9. It shows that the predicted values above  $10 \text{ m}^2 \text{ha}^{-1}$  were generally underestimating live SBA, which may be a reflection on the limited number of sites used to independently assess the allometric relationship in this value range. A paired t-test between the 44 independent sites with field-measured UMG<sub>FPC</sub> and aerial photography AP<sub>GWC</sub> estimates showed that there was no significant difference between live SBA estimated from either field or aerial photography AP<sub>GWC</sub> ( $T$  value = 1.94;  $P$ -value = 0.059;  $\alpha=0.01$ ).

## 4. Discussion

Estimates of tree biophysical parameters were extracted from very high resolution digital aerial photography captured at a GSD of 15 cm and 30 cm using OBIA. The very high spatial resolution of the digital aerial photography used in this project enabled estimates of green woody cover to be obtained over the 1 ha field sites. There was

**Table 11**

Best fit parameters for the allometric equation and summary statistics for live SBA predicted from field  $UMG_{FPC}$  and aerial derived  $AP_{GWC}$  using the allometric relationship developed between coincident field-measured live tree SBA ( $m^2 ha^{-1}$ ) and  $UMG_{FPC}$  (%).

	Allometric relationship	Predicted vs observed	
		Field measured $UMG_{FPC}$ vs observed live SBA	Aerial photography measured $AP_{GWC}$ vs observed Live SBA
Best Fit	$a = -0.32374$ $b = 1.366307$		
Parameters	$c = 0.387253$ $d = 1.366307$		
No. field sites	127	44	50
r	0.92	0.95	0.95
RMSE	2.33	2.29	2.29
Variance	5.41	5.04	5.31
Bias	0.21	0.54	0.16

a high correlation between aerial photo derived  $AP_{GWC}$  and all the woody canopy parameters assessed ( $U_{FPC}$ ,  $UM_{FPC}$ ,  $UMG_{FPC}$ , PPC and CC). The relationship between all the field-measured canopy variables and aerial derived estimates were consistent across a wide range of vegetation communities, structural classes, and across a large climate gradient, ranging from the monsoon tropics to the arid desert region. The strong relationship between all the field-based canopy parameters and aerial-derived values are likely to be due to the natural occurring relationships between these canopy attributes. Strong relationships between field-measured foliage projective cover (FPC) and CC were reported across a range of vegetation communities in the state of Queensland, Australia (Scarth et al., 2008). Scarth et al. (2008) found that FPC had a higher dynamic range than CC, saturating at around 75% and suggested that this relationship is likely to be similar elsewhere in Australia. While the number of sites used in this study with  $CC > 75\%$  were limited, a non-linear relationship between CC and  $UMG_{FPC}$  obtained from field measurements is evident (unpublished data). Armston et al. (2009) showed how woody FPC at Landsat scale could be predicted from observed densitometer measurements recording the presence and absence of green leaf along transects. This is because estimates of vegetation cover fraction, which are proportions, can generally be scaled, unlike NDVI (Zhangyan et al., 2006).

The ability to discriminate between different objects in any remotely sensed imagery is determined by the spatial and spectral

limitations of the data (Blaschke 2010; Staben et al., 2012). Accuracy assessment of the supervised classification showed that while overall accuracy for imagery captured at 30 cm GSD was higher than 15 cm imagery, accuracy of the green woody class was higher in the 15 cm imagery. For the green woody class the majority of the commission and omission error occurred between the ground layer and shadow classes. It could be assumed that the ability to resolve green from non-green components in the 30 cm GSD would become more difficult, due to the increased mixing of these components in each pixel. This increased spectral homogeneity of 30 cm pixels may have reduced the ability of the classification algorithm to spectrally separate these classes.

To enable parameters extracted from aerial photography to be used with any confidence the results need to be compared with field-measured data (Fensham and Fairfax 2007). In this study, the collection of the proportion of woody FPC for each stratum enabled the relationship between aerial-derived  $AP_{GWC}$  estimates and field-measured parameters to be better understood. The results show that parameters extracted from the 15 cm GSD aerial photography exhibited the strongest relationship with field-measured woody  $UMG_{FPC}$ . Relationships between estimates derived from imagery at GSD of 30 cm were not as clearly defined for  $UM_{FPC}$  and  $UMG_{FPC}$  with both showing statistically significant relationships. Not all field sites used in this study contained multiple strata, which can be seen in the underestimation of  $U_{FPC}$  and  $UM_{FPC}$  from the aerial

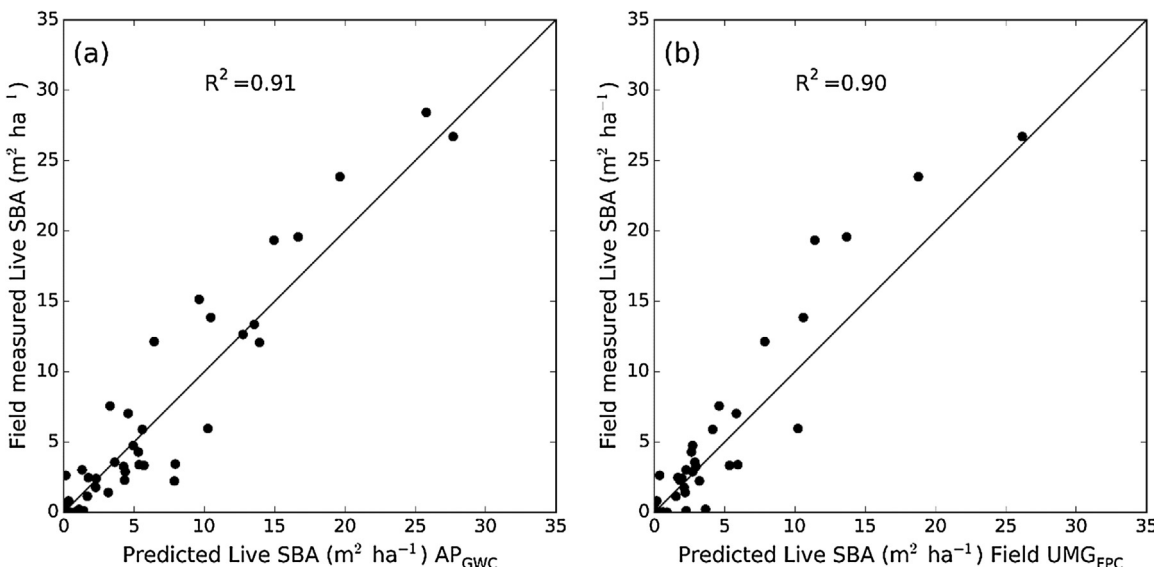


**Fig. 9.** Scatter plot showing the predicted and observed live SBA estimates, plot (a) represents the 50 sites where live SBA was predicted from  $AP_{GWC}$  and plot (b) where live SBA was predicted from 44 field-measured  $UMG_{FPC}$ .

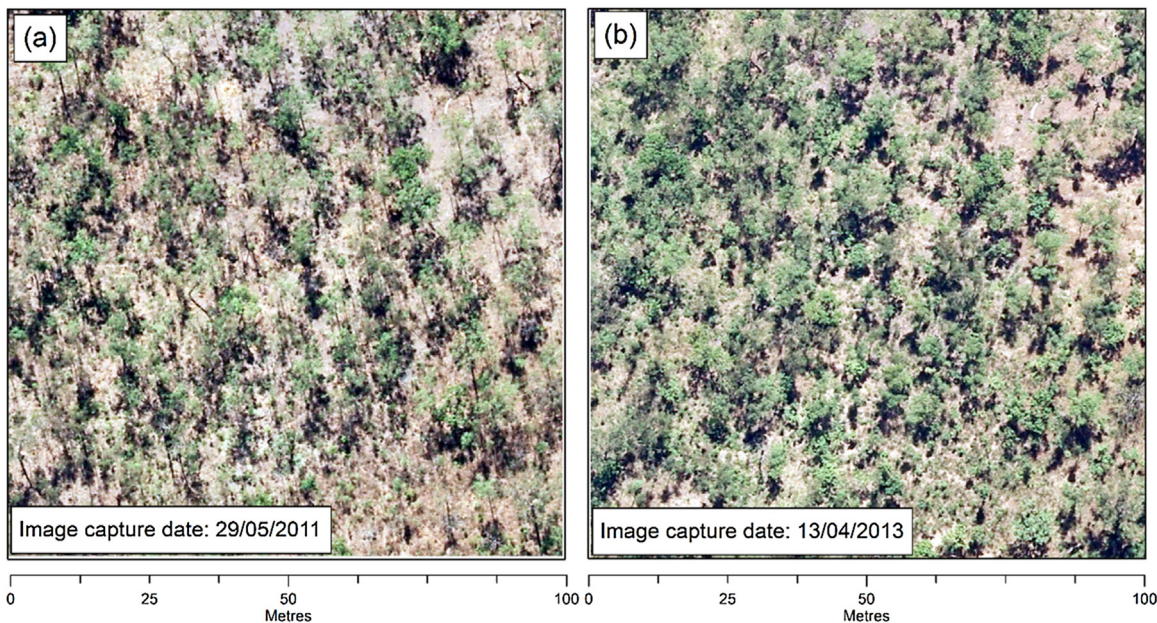


**Fig. 10.** Example of the seasonal differences in green woody vegetation captured in different date imagery (GSD 15 cm) for the same field site.

photography for both GSD 15 cm and 30 cm (Fig. 6). In a number of the sites the only woody cover present were shrubs recorded in the ground strata. The parameters derived from the aerial photographs were generally lower when compared to field measured PPC and CC. Overall there was less variance and scatter in the relationship between the field parameters and measures derived from the higher spatial resolution 15 cm GSD imagery.

It is possible that the increased scatter observed in the results for the 30 cm GSD imagery is due to the differences in the spatial resolution. Previous studies using film captured aerial photography to estimate CC from both 1:25,000 and 1:40,000 scales found that increase in photo scale resulted in overestimation of CC when compared to field-measured data (Fensham et al., 2002; Fensham and Fairfax 2007). The increased pixel size of the 30 cm imagery would lead to a reduction in the number of gaps visible in the canopy resulting in an overestimating of the green woody fraction at some sites. Examination of the scatter plots in Fig. 6 indicates that PPC was in general being underestimated by the AP<sub>GWC</sub>. This suggests something other than the non-green component of the canopy is influencing the scatter observed around the 1:1 line for UMG<sub>FPC</sub> and UMG<sub>FPC</sub>. The increased error for the 30 cm imagery may be a result of small shrubs going undetected due the reduced spatial resolution. Previous studies have shown that detection of smaller shrubs can be problematic due to the spatial resolution of the imagery used (Robinson et al., 2008; Browning et al., 2009).

Comparisons of twenty sites where imagery was captured at both GSD of 15 cm and 30 cm suggest that aerial AP<sub>GWC</sub> measures were not significantly different. While the statistical tests indicate that there was no significant difference, a number of sites varied by up to 22%. These outliers (Fig. 7) could be a result of real changes occurring at these sites due to the different image capture dates, up to 35 months in some instances. The difference observed could be due to factors such as fire which occur at these sites on a regular basis (Murphy et al., 2010) or storm events which result in wind-throw and damage to tree crowns (Staben and Evans 2008; Franklin et al., 2010). The differences in green woody vegetation may also be as a result of annual seasonal variation in FPC at these sites. Sites with the greatest difference in green woody vegetation were located in *Eucalyptus tetrodonta* and *E. miniata* dominated woodlands, which contain understoreys

of mixed species. The differences measured in the aerial photography may represent natural variation in leaf fall and leaf flush, which occurs during the year (Williams et al., 1997; O'Grady et al., 2000). Williams et al. (1997) identified four main phenological types in the Darwin region, which included evergreen, brevideciduous or partly deciduous, semi-deciduous and fully deciduous species. They reported that there were significant interannual, interspecific and intraspecific differences in leaf phenophases over the 2.5 years period of their study (Williams et al., 1997). An example of seasonal variation in green woody vegetation visible in the imagery captured at 15 cm GSD on different dates is shown in Fig. 10. Field measurements also captured the seasonal variability at this site with data collected on the 05/06/2012 and 23/05/2013 resulting in UMG<sub>FPC</sub> values of 41% and 55% respectively. This example highlights the sensitivity of the imagery to detect the changes in green woody vegetation at this site.

Some of the difference between field and image derived estimates could be due to error in the field surveys. The star transect used to measure these sites represents a sample of the woody cover over an area of 1 ha. In sites where there is a low density of tree cover it is possible that the configuration of the three 100 m transects may fail to detect individual trees, resulting in an underestimation of cover. This did occur on one site where no woody cover was measured along the three 100 m transects, however, there were clearly a number of trees visible in the imagery. While every effort is made to locate field sites in areas of homogeneous tree cover, the natural variability in the distribution of trees at a site may also result in an over or underestimation of woody cover. This is largely determined by the location of the star transect at the site, which may sample a disproportionate of either tree canopy or bare ground. This is one advantage in using aerial photography as it enables a complete census of the 1 ha plot, removing one of the limitations of the field survey in sites where there is scattered or uneven clumping of woody vegetation.

Shadow can also reduce the overall accuracy of estimates of canopy parameters from aerial photography with the shadow from taller trees obscuring adjacent lower tree canopy (Coggins et al., 2008). To reduce the impact of shadow in the imagery Coggins et al. (2008) recommended that imagery could be captured during overcast condition and during times that reduce the impact of the sun

angle. While the timing of the capture of the aerial photography used in this study is restricted to reduce the effect of the sun angle in an image, shadow did impact on the estimates of AP<sub>GWC</sub> in sites with high cover such as the monsoon rainforest. This was evident in the monsoon rainforest site for both GSD 15 cm and 30 cm, where shadows from taller trees were obscuring the canopy of lower trees reducing the overall accuracy by 13% and 16% respectively. It is also possible that the underestimation in UMG<sub>FPC</sub> in more open sites was due to shadows from taller trees obscuring woody vegetation in the mid and ground stratum. The addition of the infrared spectral band (not available in this study) would enable vegetation indices to be produced and may assist in the discrimination of green and non-green vegetation in the imagery. Standard image enhancement of the 8-bit imagery during the selection of segments to train the classification did not enable identification of vegetation within shadows. If the operator training the image classification is able to identify objects within shadow it may be possible to create an additional class to identify the fraction of green vegetation within shadow. The reduction in the radiometric resolution of the imagery limited the detection of vegetation within shadows, however, discrimination between green fractions for woody and non-woody vegetation was reasonably successful (Tables 7 and 8). While most aerial photography captured in the NT is during the dryer months when grass species are senescent, a number of the field sites used in this study contained non-woody green vegetation such as spinifex. Spinifex is a perennially green grass, which is found across large tracks of the Northern Territory (Wilson et al., 1990). Despite the limited radiometric resolution of the 8-bit data, the supervised nearest neighbour classification algorithm used in this project was able to spectrally separate the different green fractions for larger trees and non-woody spinifex species within imagery captured at 30 cm GSD. It should be noted that the method used in this study relies on the operator selecting the training samples in the imagery. If the operator selecting the training samples is not familiar with the objects visible in the imagery the results are likely to be erroneous. At one site located in the southern NT, separation of small shrubs (chenopods, height range 0.01–0.03 m) from non-woody green vegetation was not able to be achieved. In this example, the green component of the small shrub was not able to be identified in the 30 cm GSD imagery. The apparent shadow of these shrubs was visible in the imagery and classified accordingly. When the percentage of shadow in the imagery (2.97%) was compared with the woody cover measured in the field (2.33%) the results were very similar with only 0.64% difference. While the results at this site suggest that shadow was representative of the woody FPC it is likely that the green woody component of these shrubs were not able to be resolved in the 8-bit 30 cm imagery. The supervised classification method used in this study requires that the targets being classified are visible to the operator selecting the training classes. In this instance, imagery captured at a smaller GSD may enable these small shrubs to be identified and classified. Laliberte et al. (2010) reported high correlation between image-derived and field-measured shrub cover using very high resolution digital imagery captured at 4 cm GSD. They used an OBIA classification method and were able to classify all the dominant shrub species in their plots. In general, they found that the image-derived shrub cover was higher than the field-measured cover, however, for some shrub species estimates derived from the imagery were lower, possibly due to smaller shrubs (<12 cm × 12 cm) not being detected in the imagery (Laliberte et al., 2010).

The development of allometric relationships between tree structural attributes is well established (O'Grady et al., 2000; Cook et al., 2005; Williams et al., 2005; Suganuma et al., 2006; Armston et al., 2009). O'Grady et al. (2000) reported strong relationships between field-measured leaf area index (LAI) and basal area for the dominant woodland tree species *Eucalyptus tetrodonta* and *E. mini-*

*ata* in the northern half of the NT. Allometric relationships based on field-measured parameters have also been developed to predict woody FPC from SBA across the state of Queensland, Australia, with reported RMSE of 7.26% (Armston et al., 2009). Similar allometric relationships between field-measured live SBA and UMG<sub>FPC</sub> have been developed across the Northern Territory (based on 167 field sites), resulting in an RMSE of 7.48% (unpublished data). In this study, the inverse of this relationship was applied to 127 field sites to develop an allometric equation to predict live SBA from woody UMG<sub>FPC</sub> measured in the field. A number of studies have developed models to predict SBA from CC estimates derived from aerial photography (Fensham et al., 2002; Coggins et al., 2008). Coggins et al. (2008) used digital aerial photography captured at 10 cm GSD to measure canopy crown area of individual lodgepole pine trees. Prediction equations were developed between field-measured tree crown area and stem diameter (cm) from individual trees, which were applied to the crown area estimated from the aerial photography to predict stocking densities (Coggins et al., 2008).

In this study, there was very little difference between the values of the error statistics for data used to develop the allometric relationship and data used independently to assess the overall accuracy of the predicted live SBA (Table 11). While there is inherent scatter in the relationship between live SBA and UMG<sub>FPC</sub> (Fig. 8) the close agreement between live SBA values predicted from the independent validation sites from both field and aerial photographs supports the fact that UMG<sub>FPC</sub> is being accurately estimated from aerial photographs at a similar accuracy level to the field measurements. Unless there is some sort of disturbance at a site, the live SBA is not likely to change dramatically during the year. The natural seasonal variability in woody FPC values due to the presence of deciduous species is likely to be contributing to the error in the estimates of live SBA derived from the aerial photography.

The close agreement demonstrated in this study between AP<sub>GWC</sub> estimates obtained from the aerial photography and field measured UMG<sub>FPC</sub> have the potential to be used in a number of different applications, including the calibration and validation of image products derived from coarser spatial resolution satellite imagery such as Landsat. The prediction of biophysical parameters like woody FPC from coarser spatial resolution satellite imagery at a regional scale requires a significant quantity of samples representing the variability and range of woody FPC. This type of information is typically obtained from the collection of field data and represents a significant financial investment (Cohen et al., 2003). The methodology and assessment of the AP<sub>GWC</sub> estimates derived from aerial photography in this study would enable a large number of surrogate field sites to be obtained from vegetation communities across the full spectrum of woody FPC values in the Northern Territory. The use of the digital aerial photography enables sites to be randomly selected, reducing bias in site selection, reducing the risk of spatial autocorrelation, and enabling sufficient sites to be produced for comprehensive accuracy assessments. While large numbers of surrogate field sites could be obtained, the need to collect field data can never be completely replaced by the methodology developed in this study. This is highlighted by the effect of shadow in the imagery where estimates in sites with high woody cover such as monsoon forests are likely to be underestimated. Analysis of digital aerial photography with the addition of the fourth multispectral infrared band and full dynamic range may reduce this error, and requires further investigation. One of the major benefits of this study is the ability to extract biophysical parameters from the historical archive of digital aerial photography. This is particularly relevant when the satellite imagery (such as Landsat TM5) is no longer operational and field estimates are required coincident with the image overpass. The results of this study show seasonal variability in green woody vegetation could be detected in

the digital aerial photography. This sensitivity suggests that when relating biophysical parameters (derived from the aerial photography) to satellite imagery it is important to obtain satellite imagery coincident as possible with the capture date of the aerial photography.

## 5. Conclusion

The overall goal of this study was to investigate the use of digital aerial photography as a surrogate for the collection of field data. The findings of this study show that there is a strong relationship between field-measured woody UMG<sub>FPC</sub> and AP<sub>GWC</sub> derived from aerial photography captured across a broad range of vegetation communities in the Northern Territory (NT), Australia. To our knowledge this is the first study that looks at the relationship between field measured woody FPC (measured using the Australian national standard methodology), based on an extensive field dataset covering a diverse range of vegetation communities, and biophysical parameters from digital aerial photography in the NT. Statistical analysis shows that quantitative measurements of the UMG<sub>FPC</sub> can be extracted from digital aerial photography captured at GSD of 15 cm and 30 cm. Evidence of the relationship is further highlighted by the close agreement of live SBA predicted from both UMG<sub>FPC</sub> and AP<sub>GWC</sub> using allometric relationship developed from field measured data. The classification methodology presented in this paper relies on the operator's ability to identify green woody and non-green material in the imagery. Despite the reduced dynamic range (8-bit) of the aerial photography used in this project, the supervised classification of the aerial photography using an object based image analysis approach, enabled green woody components in the imagery to be quantified across a diverse range of vegetation communities. The use of aerial photography to obtain woody FPC estimates has advantages for sites with low tree density, as it samples the entire image ensuring all trees are detected. Shadow is likely to limit its use in areas with very high woody cover, however, it may be possible that imagery retaining the full dynamic range (14-bit) of the sensor and the addition of the near infrared band may enable green woody vegetation to be identified within shadow areas. The aerial photography classified in this study was subset to represent 100 m × 100 m field sites designed to be used for the calibration and validation of Landsat satellite sensors. However, it is also possible that larger areas could be classified, providing a source of calibration and validation data for other coarser spatial resolution sensors such as MODIS.

## Acknowledgments

This study would not have been possible without the support of the Northern Territory Government, in particular the Department of Land Resource Management and Department of Planning and Infrastructure. Acknowledgment goes to the many people involved in the collection of field data used in this project, Nick Cuff, Peter Brocklehurst, Jason Barnetson, Jock Duncan, Sarah Thorne, Laurie Tait, David Hooper, Ellyse Sheridan, Steele Davies, Johnelle Stevens, Tony Rosling and the many people involved in the leaf fall project undertaken by the Darwin Centre for Bushfire Research, CDU (formerly Bushfires NT). Thanks to Doug Rannard and Danielle Meehl for supply of aerial photographs and technical information in regards to the NTG aerial photography archive. Additional thanks goes to the two anonymous reviewers.

## References

- Armston, J.D., Denham, R.J., Danaher, T.J., Scarth, P.F., Moffiet, T.N., 2009. Prediction and validation of foliage projective cover from Landsat-5 TM and Landsat-7 ETM+ imagery. *J. Appl. Remote Sens.* 3, 033–540.
- Armston, J., Disney, M., Lewis, P., Scarth, P., Phinn, S., Lucas, R., Bunting, P., Goodwin, N., 2013. Direct retrieval of canopy gap probability using airborne waveform lidar. *Remote Sens. Environ.* 134, 24–38.
- Baldi, P., Brunak, S., Chauvin, Y., Andersen, C.A.F., Nielsen, H., 2000. Assessing the accuracy of prediction algorithms for classification: an overview. *Bioinformatics* 16 (5), 412–424.
- Benz, U.C., Hofmann, P., Willhauck, G., Lingenfelder, I., Heynen, M., 2004. Multi-resolution, object-oriented fuzzy analysis of remote sensing data for GIS-ready information. *ISPRS J. Photogramm. Remote Sens.* 58, 239–258.
- Blaschke, T., Hay, G.J., Kelly, M., Lang, S., Hofmann, P., Addink, E., Feitosa, R.Q., 2014. Geographic object-based image analysis—towards a new paradigm. *ISPRS J. Photogramm. Remote Sens.* 87, 180–191.
- Blaschke, T., 2010. Object based image analysis for remote sensing. *ISPRS J. Photogramm. Remote Sens.* 65, 2–16.
- Bowman, D.M.J.S., Latz, P.K., Panton, W.J., 1994. Pattern and change in an *Acacia aneura* Shrubland and *Triodia hummock* grassland mosaic on rolling hills in Central Australia. *Aust. J. Bot.* 43, 25–37.
- Bowman, D.M.J.S., Boggs, G.S., Prior, L.D., Krull, E.S., 2007. Dynamics of *Acacia aneura*-*Triodia* boundaries using carbon (14C and δ13C) and nitrogen (δ15N) signatures in soil organic matter in central Australia. *Holocene* 17 (3), 311–318.
- Brocklehurst, P., Lewis, D., Napier, D., Lynch, D., 2007. Northern Territory Guidelines and Field Methodology for Vegetation Survey and Mapping. Technical Report No. 02/2007D. Department of Natural Resources, Environment and the Arts, Palmerston, Northern Territory.
- Browning, D.M., Archer, S.R., Byrne, A.T., 2009. Field validation of 1930 aerial photography: what are we missing? *J. Arid Environ.* 73 (9), 844–853.
- Buckley, R., 1981. Soils and vegetation of central Australian sandridges II. Sandridge vegetation in the Uluru National Park Area, Northern Territory, Australia. *Aust. J. Ecol.* 6, 391–404.
- Campbell, J.B., 1996. *Introduction to Remote Sensing*, 2nd ed. The Guilford Press, New York & London.
- Carreiras, J.M.B., Pereira, J.M.C., Pereira, J.S., 2006. Estimation of tree canopy cover in evergreen oak woodlands using remote sensing. *For. Ecol. Manage.* 223 (1–3), 45–53.
- Clewley, D., Lucas, R., Accad, A., Armston, J., Bowen, M., Dwyer, J., Pollock, S., Bunting, P., McAlpine, C., Eyre, T., Kelly, A., Carreiras, J., Moghaddam, M., 2012. An approach to mapping forest growth stages in Queensland, Australia through integration of ALOS PALSAR and Landsat sensor data. *Remote Sens.* 4, 2236–2255.
- Coggins, S.B., Coops, N.C., Wulder, M.A., 2008. Initialisation of an insect infestation spread model using tree structure and spatial characteristics derived from high spatial resolution digital aerial imagery. *Can. J. Remote Sens.* 34 (6), 485–502.
- Cohen, W.B., Maiersperger, T.K., Gower, S.T., Turner, D.P., 2003. An improved strategy for regression of biophysical variables and Landsat ETM + data. *Remote Sens. Environ.* 84, 561–571.
- Congalton, R.G., Green, K., 2009. *Assessing the Accuracy of Remotely Sensed Data: Principles and Practices*, second ed. CRC Press, Taylor & Francis Group.
- Cook, G.D., Heerdegen, R.G., 2001. Spatial variation in the duration of the rainy season in monsoonal Australia. *Int. J. Climatol.* 21, 1723–1732.
- Cook, G.D., Liedloff, C., Eager, R.W., Chen, X., Williams, R.J., O'Grady, P., Hutley, L.B., 2005. The estimation of carbon budgets of frequently burnt tree stands in savannas of northern Australia, using allometric analysis and isotopic discrimination. *Aust. J. Bot.* 53 (7), 621–630.
- Coops, N.C., Delahaye, A., Pook, E., 1997. Estimation of Eucalypt forest leaf area index on the South Coast of New South Wales using Landsat MSS data. *Aust. J. Bot.* 45, 757–769.
- Cuff, N., Brocklehurst, P., 2015. Leaf and coarse fuel accumulation and relationships with attributes in 'evergreen' tropical eucalyptus savannas. In: Carbon Accounting and Savanna Fire Management. CSIRO Publishing (Chapter 7).
- Dorigo, W., Lucieer, A., Podobnikara, T., Carni, A., 2012. Mapping invasive *Falllopia japonica* by combined spectral, spatial, and temporal analysis of digital orthophotos. *Int. J. Appl. Earth Obs. Geoinf.* 19, 185–195.
- Fensham, R.J., Fairfax, R.J., 2002. Aerial photography for assessing vegetation change: a review of applications and the relevance of findings for Australian vegetation history. *Aust. J. Bot.* 50, 415–429.
- Fensham, R.J., Fairfax, R.J., 2007. Effect of photoscale, interpreter bias and land type on woody crown-cover estimates from aerial photography. *Aust. J. Bot.* 55, 457–463.
- Fensham, R.J., Fairfax, R.J., Holman, J.E., Whitehead, P.J., 2002. Quantitative assessment of vegetation structural attributes from aerial photography. *Int. J. Remote Sens.* 23 (11), 2293–2317.
- Fensham, R.J., Bray, S.G., Fairfax, R.J., 2007. Evaluation of aerial photography for predicting trends in structural attributes of Australian woodland including comparison with ground-based monitoring data. *J. Environ. Manage.* 83, 392–401.
- Foran, B.D., Cellier, K.M., 1980. An evaluation of large scale aerial photography for assessing range condition in central Australia. *Aust. Rangel. J.* 2 (2), 189–200.
- Franklin, D.C., Brocklehurst, P.S., Lynch, D., Bowman, D.M.J.S., 2007. Niche differentiation and regeneration in the seasonally flooded Melaleuca forests of northern Australia. *J. Trop. Ecol.* 23 (4), 457–457.
- Franklin, D.C., Gunton, R.M., Schatz, J., Lawes, M.J., 2010. Resprouting responses of trees in a fire-prone tropical savanna following severe tornado damage. *Austral Ecol.* 35 (6), 685–694.
- Gruber, M., Ponticelli, M., Bernögger, S., Leberl, F., 2008. UltraCamX, the large format digital aerial camera system by Vexcel Imaging/Microsoft. *Intl. Arch. Photogramm. Remote Sens. Spat. Info. Sci.* XXXVII (B1), 665–670.

- Harvey, K.R., Hill, G.J.E., 2001. Vegetation mapping of a tropical freshwater swamp in the Northern Territory, Australia: a comparison of aerial photography, Landsat TM and SPOT satellite imagery. *Int. J. Remote Sens.* 22, 2911–2925.
- Hill, G.J.E., Carter, J.L., 1999. The role of remote sensing and GIS technologies for indigenous resource management in northern Australia. *Aust. Biol. Rev.* 12, 6–12.
- Karfs, R.A., Abbott, B.N., Scarth, P.F., Wallace, J.F., 2009. Land condition monitoring information for reef catchments: a new era. *Rangel. J.* 31, 69–86.
- Laliberte, A.S., Fredrickson, E.L., Rango, A., 2007. Combining decision trees with hierarchical object-oriented image analysis for mapping arid rangelands. *Photogramm. Eng. Remote Sens.* 73 (2), 197–207.
- Laliberte, A.S., Browning, D.M., Herrick, J.E., Gronemeyer, P., 2010. Hierarchical object-based classification of ultra-high-resolution digital mapping camera (DMC) imagery for rangeland mapping and assessment. *J. Spat. Sci.* 55 (1), 101–115.
- Leberl, F., Gruber, M., 2005. Ultracam-D: understanding some noteworthy capabilities. In: D. Fritsch (Eds.), *Photogrammetric Week*. Wichmann-Verlag, Stuttgart, Germany, pp. 57–67.
- Leberl, F., Gruber, M., Ponticelli, M., Wiechert, A., 2012. The ultracam story. *Int. Arch. Photogramm. Remote Sens. Spat. Info. Sci.* XXXIX (B1), 39–44 (isprsarchives-XXXIX-B1-39-2012).
- Lewis, D., Phinn, S., Arroyo, L., 2013. Cost-effectiveness of seven approaches to map vegetation communities—a case study from northern Australia's Tropical Savannas. *Remote Sens.* 5 (1), 377–414.
- Lucas, R.M., Ellison, J.C., Mitchell, A., Donnelly, B., Finlayson, M., Milne, A.K., 2002. Use of stereo aerial photography for quantifying changes in the extent and height of mangroves in tropical Australia. *Wetlands Ecol. Manage.* 10, 159–173.
- Ludwig, J., Hindley, N., Barnett, G., 2003. Indicators for monitoring minesite rehabilitation: trends on waste-rock dumps, northern Australia. *Ecol. Indic.* 3 (3), 143–153.
- Mannel, S., Price, Z.M., Hua, D., 2006. A method to obtain large quantities of reference data. *Int. J. Remote Sens.* 27 (3), 623–627.
- McDonald, N.S., McAlpine, J., 1991. Floods and droughts: the northern climate. In: Haynes, C.D., Ridpath, M.G., Willimans, M.A.J. (Eds.), *Monsoonal Australia. Landscape Ecology and Man in The Northern Lowlands*. A. A. Balkema, Rotterdam, pp. 19–29.
- Mellor, A., Haywood, A., Stone, C., Jones, S., 2013. The performance of random forests in an operational setting for large area sclerophyll forest classification. *Remote Sens.* 5, 2838–2856.
- Morgan, J.L., Gergel, S.E., Coops, N.C., 2010. Aerial photography: a rapidly evolving tool for ecological management. *BioScience* 60 (1), 47–59.
- Muir, J., Schmidt, M., Tindall, D., Trevithick, R., Scarth, P., Stewart, J.B., 2011. *Field Measurements of Fractional Ground Cover: A Technical Handbook Supporting Ground Cover Monitoring for Australia*. Queensland Department of Environment and Resource Management for the Australian Bureau of Agricultural and Resources Economics and Sciences, Canberra.
- Murphy, B.P., Russell-Smith, J., Prior, L.D., 2010. Frequent fires reduce tree growth in northern Australian savannas: implications for tree demography and carbon sequestration. *Global Change Biol.* 16 (1), 331–343.
- Nicholas, A.M.M., Franklin, D.C., Bowman, D.M.J.S., 2009. Coexistence of shrubs and grass in a semi-arid landscape: a case study of mulga (*Acacia aneura*, *Mimosaceae*) shrublands embedded in fire-prone spinifex (*Triodia pungens*, *Poaceae*) hummock grasslands. *Aust. J. Bot.* 57 (5), 396–405.
- O'Grady, A.P., Chen, X., Eamus, D., Hutley, L.B., 2000. Composition, leaf area index and standing biomass of eucalypt open forests near Darwin in the Northern Territory, Australia. *Aust. J. Bot.* 48, 629–638.
- Pu, R., Xu, B., Gong, P., 2003. Oakwood crown closure estimation by unmixing Landsat TM data. *Int. J. Remote Sens.* 24, 4433–4445.
- Ringrose, S., Matheson, W., Matlala, C.J.S.S., O'Neill, T., Werner, P.A., 1994. Vegetation spectral reflectance along a north-south vegetation gradient in northern Australia. *J. Biogeogr.* 21, 33–47.
- Robinson, T.P., van Klinken, R.D., Metternicht, G., 2008. Spatial and temporal rates and patterns of mesquite (*Prosopis* species) invasion in Western Australia. *J. Arid Environ.* 72 (3), 175–188.
- Rosso, P.H., Klonus, S., Ehlers, M., Tschach, E., 2008. Comparative properties of four airborne sensors and their applicability to land surface interpretation. *Int. Arch. Photogramm. Remote Sens. Spat. Info. Sci.* XXXVII (B1).
- Samani Majd, A.M., Bleiweiss, M.P., DuBois, D., Shukla, M.K., 2013. Estimation of the fractional canopy cover of pecan orchards using Landsat 5 satellite data, aerial imagery, and orchard floor photographs. *Int. J. Remote Sens.* 34 (16), 5937–5952.
- Scarth, P., Armston, J., Danaher, T., 2008. On the relationship between crown cover, foliage cover and leaf area index. In: *Proceedings of the 14th Australasian Remote Sensing and Photogrammetry Conference*, Darwin, Australia, October 2008.
- Scarth, P., Roder, A., Schmidt, M., 2010. Tracking grazing pressure and climate interaction? the role of Landsat fractional cover in time series analysis. *Proceedings of the 15th Australasian Remote Sensing and Photogrammetry Conference*, 13th–17th September 2010.
- Sharp, B., Bowman, D.M.J.S., 2004. Net woody vegetation increase confined to seasonally inundated lowlands in an Australian tropical savanna, Victoria River District, Northern Territory. *Austral Ecol.* 29, 667–683.
- Staben, G.W., Evans, K.G., 2008. Estimates of tree canopy loss as a result of Cyclone Monica, in the Magela Creek catchment northern Australia. *Austral Ecol.* 33, 562–569.
- Staben, G.W., Pfitzner, K., Bartolo, R., Lucieer, A., 2012. Empirical line calibration of WorldView-2 satellite imagery to reflectance data: using quadratic prediction equations. *Remote Sens. Lett.* 3 (6), 521–530.
- Stumpf, K.A., 1993. The estimation of forest vegetation cover descriptions using a vertical densitometer. In: *Presented at the Society of American Foresters National Convention*, Indianapolis, IN, November 8–10.
- Suganuma, H., Abe, Y., Taniguchi, M., Tanouchi, H., Utsugi, H., Kojima, T., Yamada, K., 2006. Stand biomass estimation method by canopy coverage for application to remote sensing in an arid area of Western Australia. *For. Ecol. Manage.* 222, 75–87.
- Trimble eCognition Developer 8.9 User Guide. München: Germany Trimble Documentation.
- Walker, J., Hopkins, M.S., 1990. *Australian soil and land survey: field handbook*. In: McDonald, R.C., Isbell, R.F., Speight, J.G., Walker, J., Hopkins, M.S. (Eds.), *Australian Soil and Land Survey: Field Handbook*. CSIRO, Canberra.
- Wallace, J., Behn, G., Furby, S., 2006. Vegetation condition assessment and monitoring from sequences of satellite imagery. *Ecol. Manage. Restor.* 7, 31–36.
- Whiteside, T.G., Boggs, G.S., Maier, S.W., 2011. Comparing object-based and pixel-based classifications for mapping. *Int. J. Appl. Earth Obs. Geoinf.* 13 (6), 884–893.
- Williams, R.J., Myers, B.A., Muller, M.J., Duff, G.A., Eamus, D., 1997. Leaf phenology of woody species in a northern Australian tropical savanna. *Ecology* 78, 2542–2558.
- Williams, R.J., Zerihun, A., Montagu, K., Hoffman, M., Hutley, L.B., Chen, X., 2005. Allometry for estimating above-ground tree biomass in tropical and subtropical eucalypt woodlands: towards general predictive equations. *Aust. J. Bot.* 53, 607–619.
- Wilson, B.A., Brocklehurst, P.S., Clark, M.J., Dickinson, K.J.M., 1990. *Vegetation survey of the Northern Territory*, Technical Report No. 49. Conservation Commission of the Northern Territory, Darwin.
- Wulder, M.A., White, J.C., Fournier, R.A., Luther, J.E., Magnussen, S., 2008. Spatially explicit large area biomass estimation: three approaches using forest inventory and remotely sensed imagery in a GIS. *Sensors* 8, 529–560.
- Wulder, M.A., White, J.C., Coggins, S., Ortlepp, S.M., Coops, N.C., Heath, J., Mora, B., 2012. Digital high spatial resolution aerial imagery to support forest health monitoring: the mountain pine beetle context. *J. Appl. Remote Sens.* 12 (6) (062527-1–062527-10).
- Xu, B., Gong, P., Pu, R., 2003. Crown closure estimation of oak savannah in a dry season with Landsat TM imagery: comparison of various indices through correlation analysis. *Int. J. Remote Sens.* 24 (9), 1811–1822.
- Zar, J.H., 1984. *Biostatistical Analysis*, second ed. Prentice-Hall, Inc., Englewood Cliffs, New Jersey (07632).
- Zhangyan, J., Alfredo, R.H., Jin, C., Yunhao, C., Jing, L., Guangjian, Y., Xiaoyu, Z., 2006. Analysis of NDVI and scaled difference vegetation index retrievals of vegetation fraction. *Remote Sens. Environ.* 101 (3), 366–378.